

Article Information



Article Type:	report
Journal Title:	Journal of Sustainable Cement-Based Materials
Publisher:	Taylor & Francis
DOI Number:	10.1080/21650373.2023.2246068
Volume Number:	0
Issue Number:	0
First Page:	1
Last Page:	12
Copyright:	© 2023 Informa UK Limited, trading as Taylor & Francis Group
↑	

Long-term corrosion performance and monitoring for service life estimation of LC3 concrete systems

Left running head: S. Rengaraju and R. G. Pillai

Short title : Journal of Sustainable Cement-Based Materials

[AQ0](#)



Sripriya Rengaraju^a and Radhakrishna G. Pillai^a



^aDepartment of Civil Engineering, Indian Institute of Technology Madras, Chennai, Tamil Nadu, India

Corresponding Author

Corresponding author. Email: raju.sripriya@gmail.com [AQ1](#)

The performance of quenched and self-tempered (QST) steel bars embedded in concretes with Limestone calcined clay cement (LC3), fly ash (70% OPC and 30%fly ash – PFA), and traditional OPC was assessed in severe chloride environments. Additionally, the performance of commercially available, calcium nitrite-based inhibitors in the three binder systems was also evaluated. The specimens were subjected to an alternate wet-dry cycle using the ASTM G109 test method. The findings show that LC3 concrete performs better than the OPC and PFA systems with and without inhibitors. Furthermore, when the surface resistivity, ρ , is more than 37 k Ω .cm, the concrete has high ionic resistance and the macrocell current across the two rebars could not be established as described in ASTM G109 test method. This highlights the limitations of the ASTM G109 test method and the need for more sophisticated testing methods for assessing steel corrosion in highly resistive cementitious systems.

Keywords

limestone calcined clay cement; chlorides; corrosion; macrocell specimens; resistivity; concrete



Note: Any change made here needs to be made in the corresponding section at the end of the article.

Limestone Calcined Clay (LC3) project – Phase I 7F-08527.02.01

Department of Science and Technology 10.13039/100021014 EMR/2016/003196

Ministry of Education, Government of India, through Indian Institute of Technology Madras (IITM),

Institute of Eminence Research Initiative Grant on Technologies for Low Carbon and Lean Construction (TLC2)

This research is partially funded by the Limestone Calcined Clay (LC3) project – Phase I (Project Number: 7F-

08527.02.01) sponsored by the Swiss-Agency for Development and Cooperation, Switzerland. The authors also acknowledge the financial support received from the Department of Science and Technology (Sanction No.

EMR/2016/003196) and the Ministry of Education, Government of India, through Indian Institute of Technology Madras (IITM), Chennai. The support through the Institute of Eminence Research Initiative Grant on

Technologies for Low Carbon and Lean Construction (TLC2) from IIT Madras is acknowledged.

1. Introduction

Recently, limestone calcined clay cement (LC3) has gained popularity as an alternative to traditional cement OPC due to (i) abundance of raw materials required, (ii) excellent short-term performance in laboratory studies, (iii) possibility of industrial scale-up, and (iv) up to 40% reduction of CO₂ emissions [18, 19, 43, 44]. For its wider adoption, LC3 needs to be assessed for its durability, especially long-term performance against chloride-induced corrosion, the major deterioration mechanism in most reinforced concrete structures. Hence, in this study, LC3 was assessed for its long-term performance in severe chloride environments using the standard test method ASTM G109 and the destructive chloride analysis at the end of testing.

1.1. Novel cementitious systems and chloride resistance

In recent years, many novel concrete materials claiming durability and long-term performance are coming into the market. However, the lack of standard short-term test methods, erroneous or inappropriate interpretation of data, and poor understanding of associated deterioration mechanisms often pose significant challenges for the broader adoption of these materials. Some of the challenges are discussed here.

1.1.1. Chloride resistance of steel-concrete (S-C) systems

The cover concrete is responsible for durability, resisting the transport of deleterious elements and chloride-induced corrosion. Traditionally, the chloride resistance of concrete is evaluated using test methods such as ASTM C1202, ASTM C1556, NT Build 443, and NT Build 492 and projected as the input parameters for service life estimation [9, 10, 34, 35]. The presence of supplementary cementitious materials (SCM) such as fly ash, slag, and metakaolin results in refined pore structure and denser cementitious matrix. When limestone is also present, it acts as nucleation sites and the degree of reaction of clinker and SCMs increases, especially in limestone calcined clay cement systems [14, 15, 27]. In addition, the formation of carboaluminate phases in the presence of limestone can bind the chlorides and reduce the amount of free chlorides in the pore solution. Maraghechi et al. 2019 reported high chloride resistance in LC3 due to the refined pore structure and bound chlorides [33]. However, such pore structure can lead to highly tortuous path and highly variable chloride in Steel-Concrete (S-C) interface (Angst and Polder, 2014) [6]. This variability in combination with lower alkalinity may be susceptible to pitting corrosion,

especially in metakaolin based S-C systems, despite its higher chloride resistance and longer time to initiate corrosion [29]. Moreover, these test methods account for bulk properties of concrete, which are remarkably different from the cover properties of concrete due to the occurrence of bleeding channels, curing conditions, and the presence of an interface between steel and concrete. Because of these, the service life of reinforced concrete structures is often overestimated when the input parameters are solely based on bulk concrete properties. On the other hand, the chloride threshold (Cl_{th}), which is the chloride concentration required for the initiation of corrosion of steel, is often found in the aqueous solution to shorten the testing time (Diamond, 1986) [5, 13, 20, 24, 28, 30, 36, 42, 46]. However, corrosion initiation depends on the S-C interface, which in turn depends on both the steel and concrete properties [5] (RILEM-TC-262-SCI). Hence, the Cl_{th} of steel in aqueous solution differs significantly from the S-C systems due to the presence of the interface, which buffers alkalinity by the dissolution of calcium hydroxide [32, 33]. In addition, the nature of the interface (porosity, resistivity, and pH) depends on the type of binder, water-binder ratio (w/b) used, and the presence of corrosion inhibitors, and hence influences the corrosion initiation [2]. Therefore, it is necessary to test the chloride-induced corrosion in the S-C system to assess the service life of reinforced concrete structures.

1.1.2. Electrochemical test methods for long-term performance

Half-cell potential is the most used testing technique or parameter for performance assessments in the field, which is the potential difference measured between the reference electrode and the steel embedded in concrete. However, the half-cell potential measured in novel S-C systems need not follow the absolute values defined for traditional S-C systems as per ASTM C876 [11] due to the variations in the internal moisture level and the resistivity of the cementitious matrix in the cover region. Additionally, cover thickness, steel microstructure, and the coating on steel, if any, influence the half-cell potential, and hence, the ASTM C876 cannot be adopted for all the exposure conditions (Gulikers et al. 2003, RILEM-TC-154-EMC) [3, 21, 25, 37]. Hence, in novel S-C systems, instead of absolute values, a significant reduction in potential (say, by about 150 mV) is used by many researchers as a criterion for corrosion initiation and the corresponding chloride concentration has been reported as Cl_{th} [7, 17, 31, 41] (RILEM-TC-235). Though perceived as a simple method, this possesses several challenges in practice. It can detect only when significant corrosion has occurred (to be even able to see with visible eyes when autopsied); and not as soon as the corrosion has initiated. Moreover, the short-term test methods employed such as impressed current corrosion affects the corrosion initiation mechanism when highly resistive cementitious systems are used [40]. Hence, in this paper, long-term performance of steel embedded in LC3 is evaluated using wetting and drying to understand its chloride resistance.

ASTM G109 [12] is widely used to monitor the possible macrocell corrosion mechanisms in conventional S-C systems. The ASTM G109 specimen consists of three rebars – one near the exposure region, which acts as an anode, and the two bottom rebars, which act as the cathode (See Figure 2). The macrocell voltage drop across a 100 Ω resistor between the anode and cathode is measured at regular intervals. When the cumulative macrocell charge calculated according to ASTM G109 is greater than 150 C, the corrosion is defined to be initiated, and the chloride concentration at the S-C interface is reported. This method is advantageous due to its simplicity in casting and exposure conditions. It has been mentioned that macrocell current flow between adjacent anode and cathode bars could be inhibited because of high resistivity of concrete but does not include range [8, 16, 22, 26]. However,

it is not clearly understood whether the test method is valid for novel S-C systems concrete with high ionic resistance (say, SCM-based systems).

To summarize, testing the properties of concrete alone cannot ensure the long-term performance of novel steel-concrete systems. The corrosion performance of steel in such systems needs to be assessed considering the intricacies and properties of S-C interface and cover concrete. Hence, in this paper, ASTM G109 test method is used to assess the long-term performance of LC3 and the resistivity range in which this test method is applicable is also discussed.

2. Research significance

Limestone Calcined Clay Cement (LC3) has gained significant visibility worldwide due to its low carbon footprint and superior performance in durability indicators such as moisture and chloride transport properties. To overcome the adoption barriers in case of using LC3 in reinforced concrete systems, it is now necessary to ascertain the long-term corrosion resistance of steel in LC3 systems. Moreover, the true sustainability of novel cementitious systems is established when their long-term corrosion resistance is assured in different environments. Hence, this paper presents the long-term corrosion performance of steel in LC3-based concrete exposed to severe chloride environments. In addition, the paper suggests adopting the ASTM G109 test method based on the resistivity of concrete, which is a gap in the literature. The findings are significant to the researchers and the practicing engineers in bringing novel materials from the lab-to-field.

3. Methodology

Three binders, namely OPC, PFA, and LC3 (See [Table 1](#) for composition) with the PFA system consisting of 70% OPC and 30% Class F fly ash, and the LC3 system consisting of 50% OPC clinker, 31% calcined clay, 15% limestone, and 4% gypsum, were used. The LC3 used was from an industrial trial production, which contained clay (58% Kaolinite content) from Gujarat, India [[23](#)]. Quenched and self-tempered (QST) steel (also known as TMT – Thermo Mechanically Treated steel in India) was used for this study (See [Table 2](#) for composition). The effect of corrosion inhibitors was also studied by admixing a commercial calcium nitrite-based inhibitor (proprietary dual mechanism corrosion inhibiting admixture) with 25% solid content in the OPC, PFA, and LC3 systems. Two dosages – recommended dosage (RD) by the manufacturer (5 l/m^3) and a higher dosage than the RD (20 l/m^3) were used. A total of 54 specimens were cast (See [Figure 1](#)), with six specimens for each combination as listed in [Table 3](#).

Figure 1. ASTM G109 specimens being exposed. [+](#)



Note: Figure Replacement Requested. [↓](#)

Note: The table layout displayed in 'Edit' view is not how it will appear in the printed/pdf version. This html display is to enable content corrections to the table. To preview the printed/pdf presentation of the table, please view the 'PDF' tab.

Table 1. Oxide composition of the binders used. [+](#)

Oxides	Concentration (%)	
	Limestone calcined clay cement (LC3)	


	OPC	Class F fly ash	Clinker	Calcined clay	Limestone
Al ₂ O ₃	4.17	29.95	5.24	24.95	1.74
CaO	64.59	1.28	63.81	0.09	48.54
Fe ₂ O ₃	3.89	4.32	3.41	5.08	1.62
K ₂ O	0.59	1.44	0.19	0.21	0.13
MgO	0.88	0.61	3.06	0.19	0.467
Na ₂ O	0.16	0.16	0.32	0.05	–
SiO ₂	19.01	59.32	21.12	58.43	10.07
SO ₃	1.7	0.16	0.63	–	0.01
TiO ₂	0.23	0.206	–	0.10	1.41
LOI	1.4		0.98	9.58	37.09

Place the cursor position on table column and click 'Add New' to add table footnote.

Note: The table layout displayed in 'Edit' view is not how it will appear in the printed/pdf version. This html display is to enable content corrections to the table. To preview the printed/pdf presentation of the table, please view the 'PDF' tab.

Table 2. Chemical composition of steel used. +


Element	Composition (%)
C	0.25
Si	0.378
Mn	0.66
P	0.02
S	0.017
Cr	0.058
Ni	0.032
Cu	0.016
Al	< 0.008
B	< 0.001
Nb	0.05
Pb	< 0.02

Ti	0.005
W	< 0.005
N	0.007
Fe	98.492
Total*	99.985
*Excluding other trace elements 	

Note: The table layout displayed in ‘Edit’ view is not how it will appear in the printed/pdf version. This html display is to enable content corrections to the table. To preview the printed/pdf presentation of the table, please view the ‘PDF’ tab.

Table 3. Test groups and mix designs of specimens tested. 

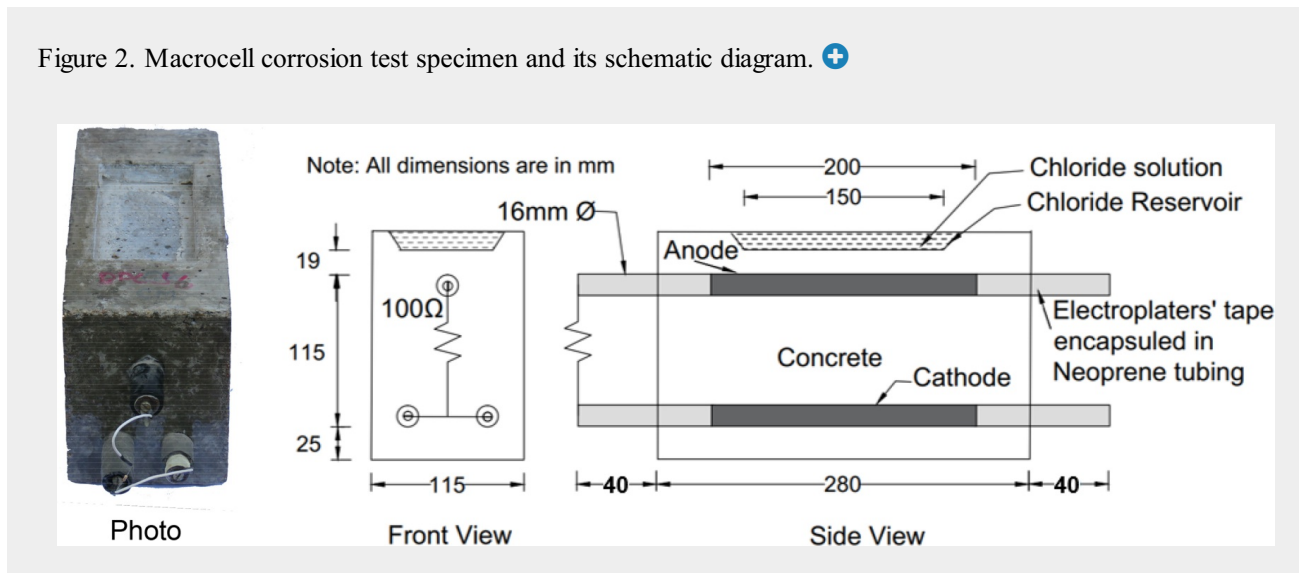
Mix ID	Binder (kg/m ³)	w/b	Fine aggregates (kg/m ³)	Coarse aggregates (kg/m ³)	Inhibitor dosage (liters/m ³)	Number of specimens
OPC-Control	360	0.5	897	964	0	6
OPC-RD					5	6
OPC-HD					20	6
PFA-Control	360	0.5	896	964	0	6
PFA-RD					5	6
PFA-HD					20	6
LC3-Control	360	0.5	888	964	0	6
LC-RD					5	6
LC3-HD					20	6

Notes: RD: Recommended Dosage of corrosion inhibitor (by the manufacturer); HD: Maximum or high dosage recommended by the manufacturer. 


3.1. Specimen preparation

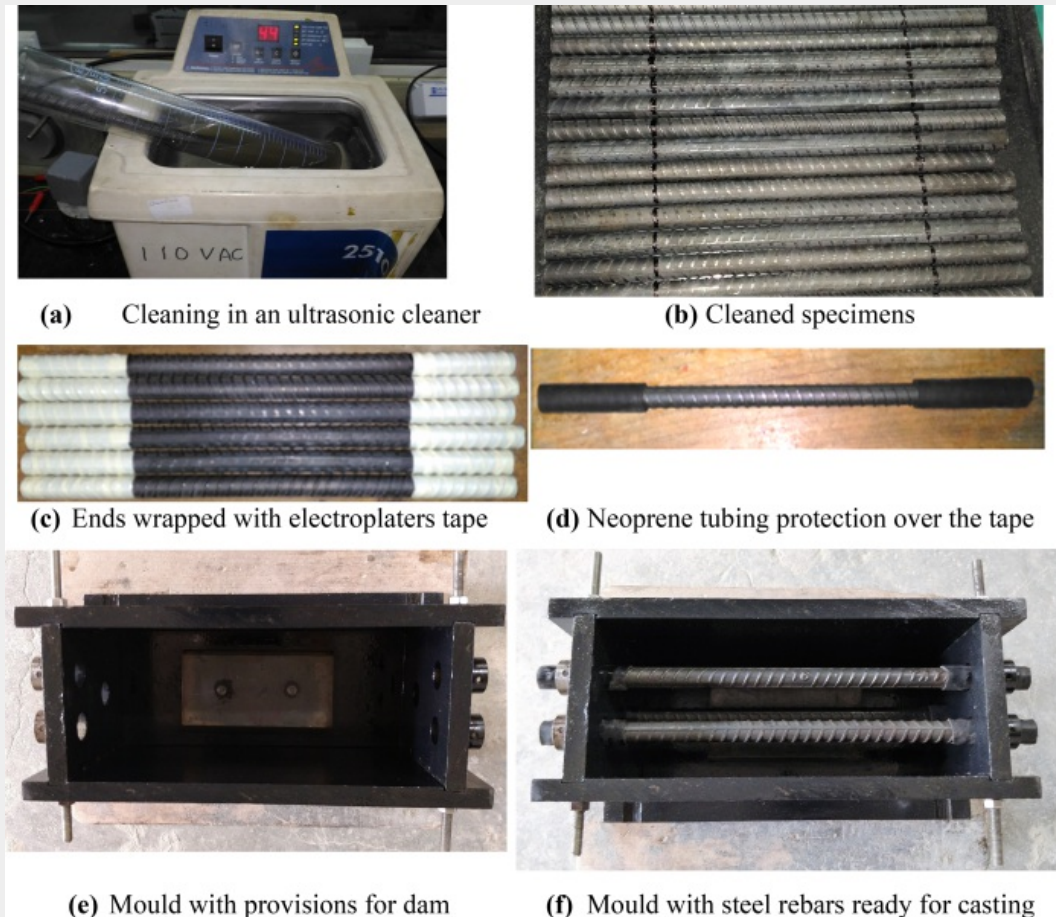
Figure 2 shows the photograph and schematic of the ASTM G109 specimen with a built-in reservoir for placing chloride solution. Table 3 shows the mix design of the concrete used. The binder content was kept the same for all the mixes to realize the benefits of SCMs. The size of the coarse aggregate was restricted to 10 mm to have a reduced cover depth of 19 mm as per the standard.

Figure 2. Macrocell corrosion test specimen and its schematic diagram. 



As shown in [Figure 3](#), TMT/QST steel pieces of 16 mm diameter were used for this study. The steel pieces of 360 mm length were cut using an abrasive cutter. The surface of the rebar was cleaned using ethanol in an ultrasonic cleaner, as shown in [Figure 3\(a\)](#); and wiped clean using a cloth. The 200 mm portion at the center of the steel rebar was marked for exposure region ([Figure 3\(b\)](#)), and the remaining were covered with electroplaters tape, see [Figure 3\(c\)](#) and then by neoprene tubing, see [Figure 3\(d\)](#). A tapered acrylic plate was attached to the bottom of the mould and the specimens were cast upside down (see [Figure 3\(e,f\)](#)) to make a provision for a chloride reservoir, to prevent the plastic settlement and bleeding water channels in the cover during casting, and to prevent leakage from the reservoir later during the monitoring phase. The monolithically cast specimens were cured in a mist room for 28 days at 25 °C and 95% RH approximately. A 100 Ω resistor was connected between the top (anode) and bottom bars (cathode) using 4 mm diameter screws to measure the voltage difference across the anode and cathode rebars.

Figure 3. Step-by-step procedure shown for casting ASTM G109 test specimen. 



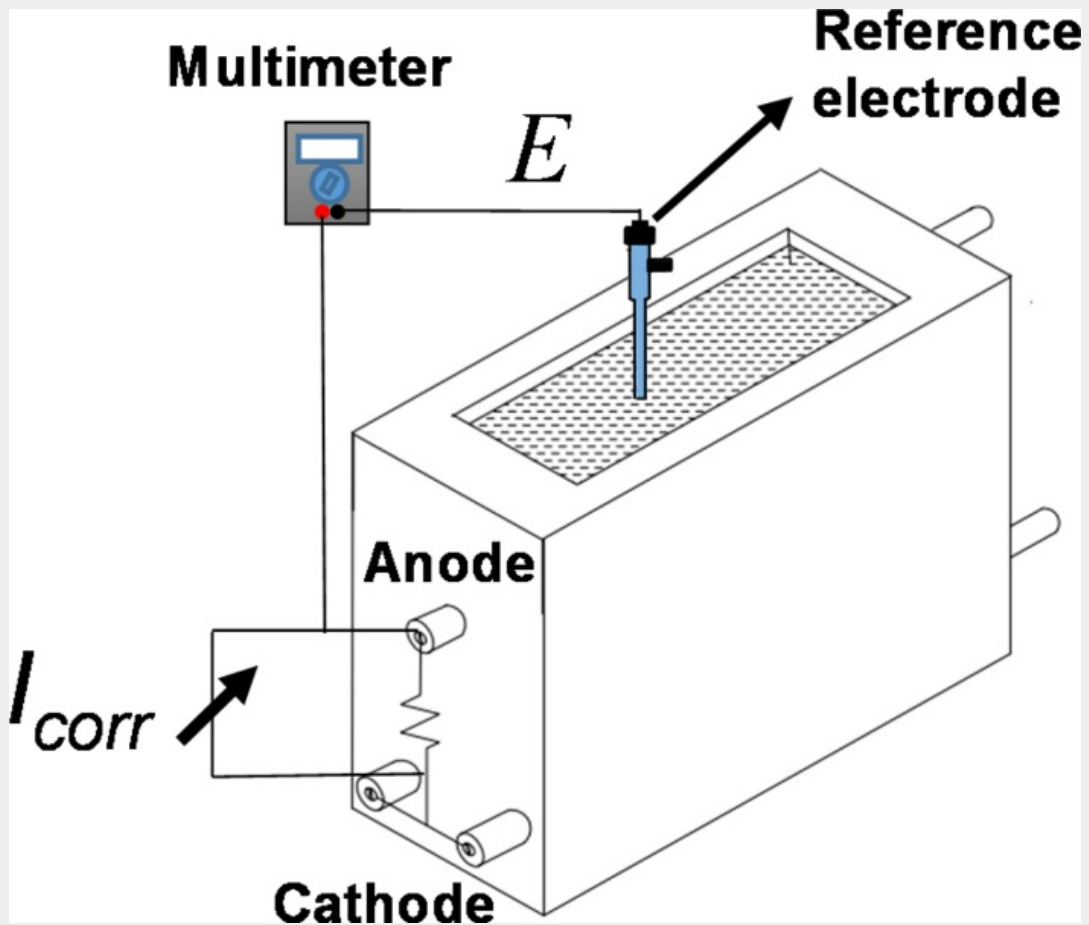
3.2. Chloride exposure and corrosion monitoring

After 28 days of curing, the specimens were surface dried, epoxy coated on the concrete surface except for top and bottom and left for 14 days. The epoxy coated specimens were then subjected to cyclic wet-dry exposure (14 days of ponding followed by 14 days of drying) using a 3% sodium chloride solution. [Figure 4](#) shows the arrangement for measuring half-cell potential (HCP) and macrocell current (I_{corr}) in ASTM G109 specimens. The voltage across the 100 Ω resistor (i.e. in the circuit established between the top and bottom rebars through concrete – Circuit 1) was measured using a 5.5-digit precision multimeter on the 7th day of wetting in each cycle. The End of Testing (EoT) was defined as the time when TC_j attains 150 Coulombs (as per the ASTM G109) using [Equation \(1\)](#)

$$TC_j = TC_{j-1} + \left[(t_j - t_{j-1}) \times \frac{i_j + i_{j-1}}{2} \right]$$

where TC = Total corrosion (Coulombs); t_j = Time of measurement of the macrocell current (seconds); and i_j = Macrocell current (Amps) at t_j . If $i_j > zero$ (i.e. i_j has positive current values), then i_j is considered as zero. The time to corrosion (days) is reported as the time when TC_j attained 150 Coulombs. In addition, the half-cell potential of the top rebar was monitored as per ASTM C876 with respect to the saturated calomel electrode (SCE). At the end of exposure/testing, all the specimens were autopsied and the anode rebars were visually observed for corrosion spots.

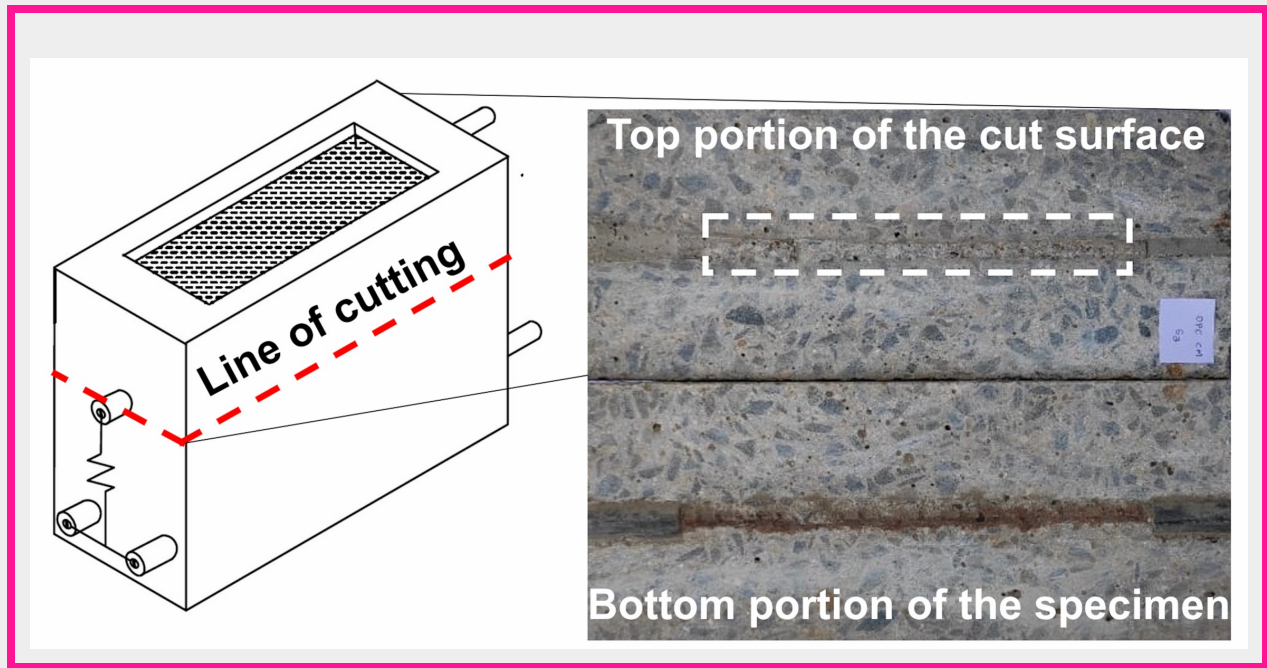
Figure 4. Set-up for half-cell potential and macrocell corrosion tests in ASTM G109 specimen. 



3.3. Determination of chloride concentration

The concrete powder was collected using a filer from the exposed region at the top piece of the autopsied specimen, where the impression of steel ribs was present as shown in [Figure 5](#). Care should be taken such that the powder collection should not go beyond 2 mm depth along the impression of the steel rebar. The collected powder was subjected to chloride analysis as per SHRP 330 [\[45\]](#)(acid-soluble chloride) to determine the chloride concentration. This value of the chloride concentration is reported as the chloride threshold (by % weight of binder).

Figure 5. Autopsied specimen showing the location for concrete powder collection. +



Note: Figure Replacement Requested.

 Slide5Fig_F005.jpeg

4. Results and discussion

This section presents the discussion on the electrochemical readings of OPC, PFA, and LC3 specimens followed by the effect of resistivity on the electrochemical circuit in highly resistive concrete systems. Thereafter, the chloride concentration at the interface of the autopsied OPC, PFA and LC3 specimens is reported.

4.1. OPC specimens

Figure 6(a–c) show the half-cell potential and macrocell corrosion voltage of OPC control specimens with a dosage of zero, RD, and HD of the inhibitor, respectively. The electrochemical readings obtained from OPC specimens clearly show that specimens with inhibitor perform better than those without inhibitor, which got corroded in less than 250 days of testing. The electrochemical readings show a steady drop in the potential and gradual increase in macrocell corrosion current in the OPC specimens. This is because of the ionic conductivity established through the concrete between the top and bottom rebars, which completes Circuit 1 (See Figure 8) as described in ASTM G109 standard (i.e. decrease in half-cell potential and increase in the macrocell current

indicating the ongoing corrosion). A higher inhibitor dosage (e.g. first HD specimen corroded at about 650 days) seemed to prolong the corrosion initiation than the recommended dosage (first RD specimen corroded at about 315 days) by about twice the time. Figure 7(a) shows the typical corrosion in the embedded rebar in OPC at the end of testing, which is the attainment of 150 C. It should be noted that the OPC-HD specimen in Figure 7(a) had lesser corrosion visually when compared to OPC-RD and OPC-control. [Please note that the deep dark rust color in OPC-HD specimen is due to the presence of moisture and the photo was taken just after cutting of specimens]. In addition to these observations, it is to be noted that the resistivity of OPC concrete is low, which was measured and plotted in Figure 13. Overall, the presence of inhibitor in OPC specimens was beneficial in extending the corrosion initiation time. The dual mechanism (protection of both anodic and cathodic sites) of the inhibitors could have prevented the corrosion initiation. The higher dosage of inhibitor increased the average corrosion initiation time by five times in comparison to control specimens without inhibitor and three times in comparison to recommended dosage.

Figure 6. Half-cell potential and macrocell corrosion current of OPC – ASTM G109 specimens. [AQ11](#)

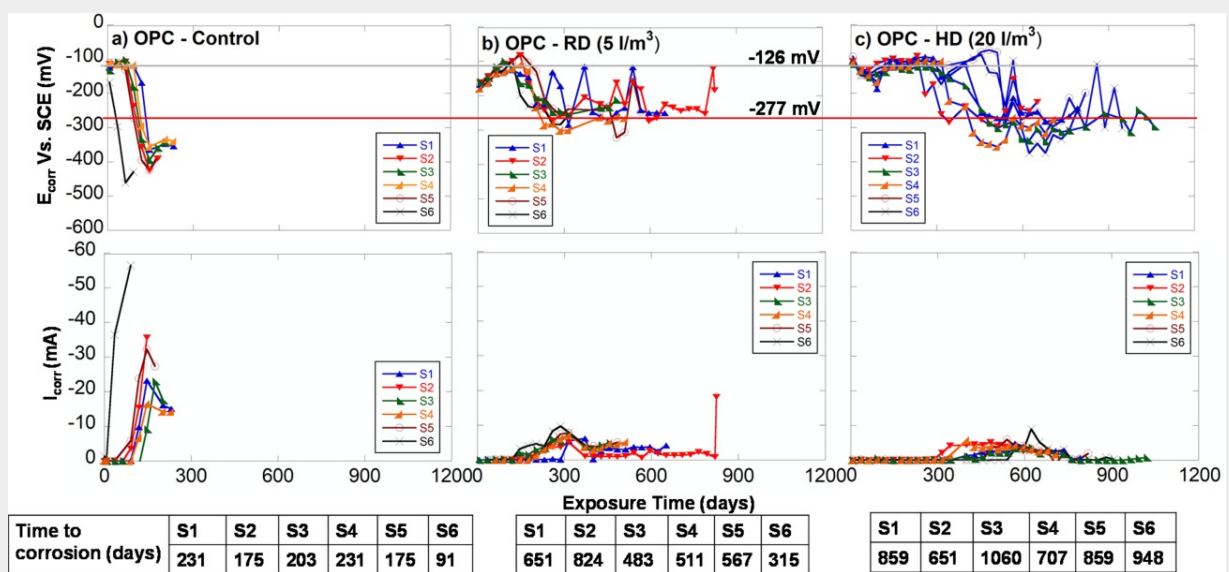

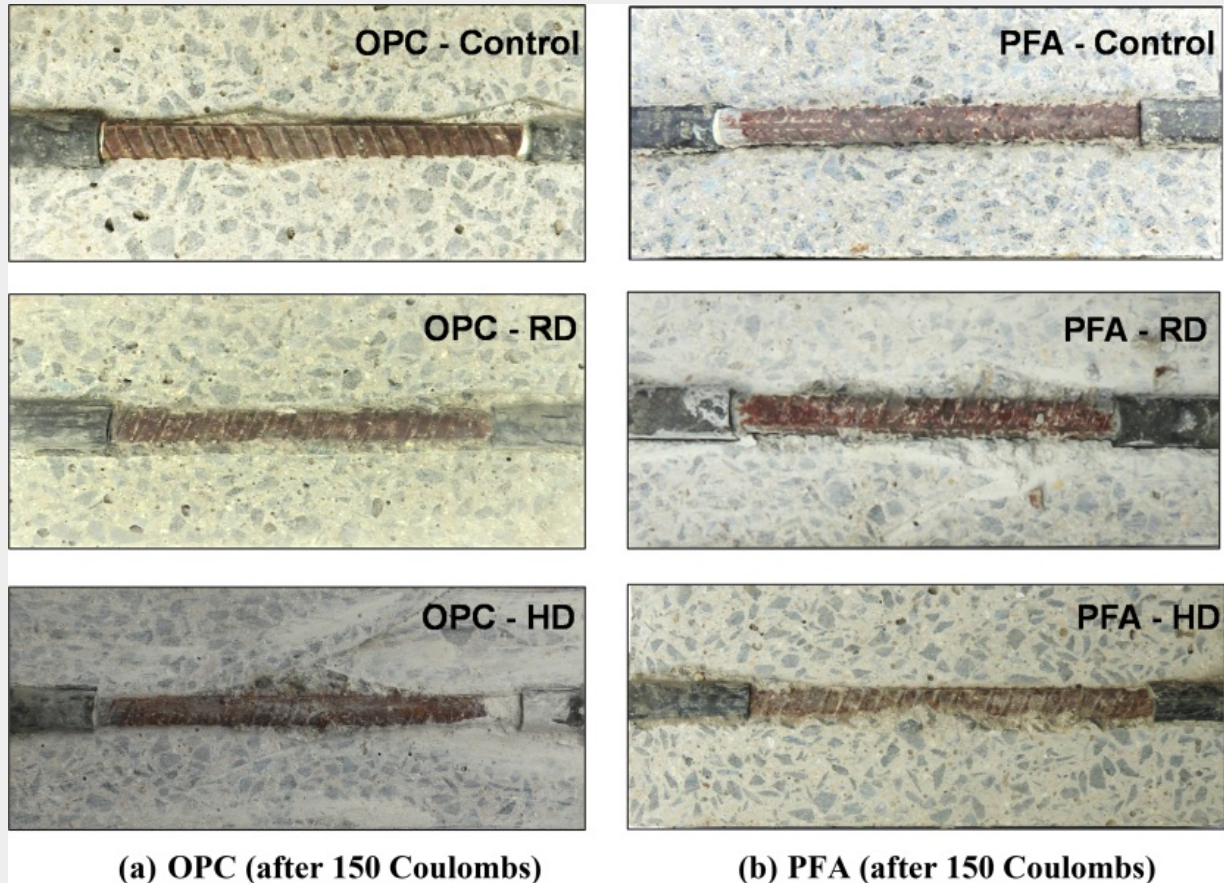


Figure 7. Typical autopsied specimens showing corrosion levels: (a) OPC specimens after attaining 150 Coulombs, (b) PFA specimens after attaining 150 Coulombs. 



4.2. PFA specimens

Figure 9(a–c) show the half-cell potential and macrocell corrosion voltage of PFA control specimens without inhibitor, with RD and HD of the inhibitor respectively. Figure 9(a) indicates that some of the specimens behaved like OPC specimens at the early age due to the slow hydration nature and corroded early in less than 200 days (S1, S2, and S3). There is a drop in potential and an increase in macrocell corrosion current in these specimens. However, as hydration evolved, some specimens (S3, S5, and S6) gained enough resistivity and prevented the ingress of chloride ions. Because of this gain in resistivity, the specimens had a more extended corrosion initiation period. In general, PFA-control specimens had better performance than OPC-control specimens. Figure 9(b,c) show that the addition of a higher dosage has no significant effect on the corrosion initiation period in PFA specimens (the first specimen corroded at about 500 days of testing) and behaves like specimens with RD. At about 300 days, there is an indication of a drop in potential in both RD and HD specimens. Interestingly, the electrochemical readings in PFA specimens with inhibitors (RD and HD) had poor behavior compared to OPC

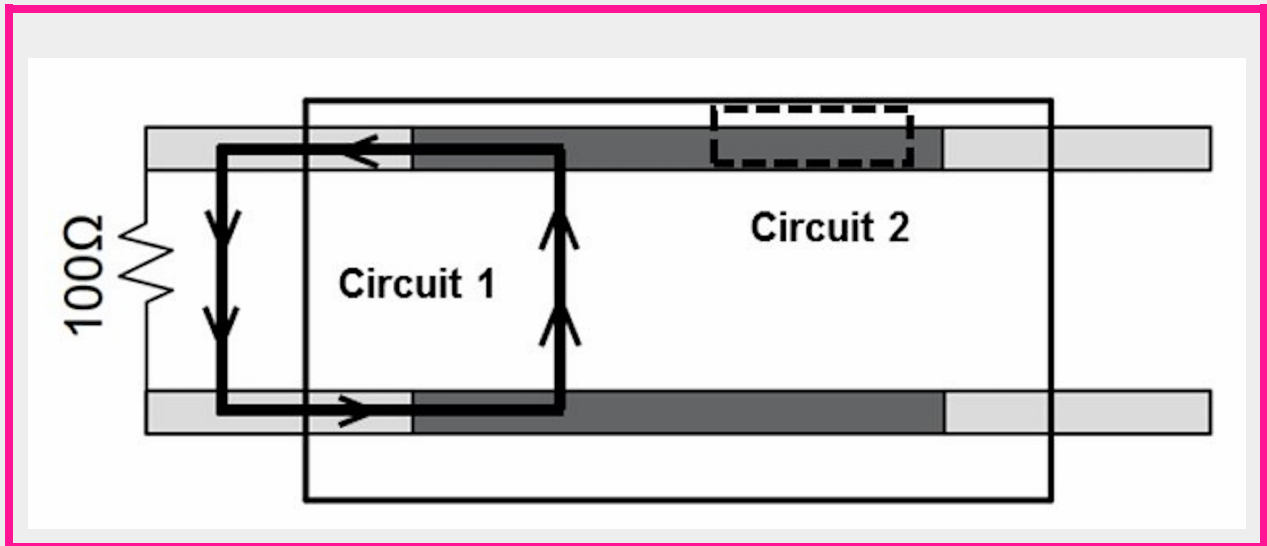
specimens with inhibitors (OPC-HD), which had a 30% longer time to corrosion. This could be due to the incompatibility of the inhibitor with PFA cement, which could have led to a poorly developed microstructure. Despite the poor electrochemical readings, the visual observation in typical PFA-HD specimens had lesser corrosion than the standard OPC-HD specimens at the end of testing, when TC_j is 150 C (See [Figure 7\(b\)](#)). This could be due to the refined microstructure that occurred due to the hydration process and the resistivity development at a later stage. The electrochemical readings in these specimens show that the necessary ionic conductivity is established at the initial stage and follows Circuit 1 as anticipated by the ASTM G109 standard.

In short, the refinement of pore structure is essential for preventing chloride ingress prevention and extending the corrosion initiation time. If the hydration is delayed, the beneficial effect could not be realized in PFA based concrete. The presence of inhibitor did not affect the corrosion initiation time significantly, which could be due to incompatibility as described earlier.

4.3. LC3 specimens

[Figure 8\(a-e\)](#)[Figure 10\(a-c\)](#) show the half-cell potential and macrocell corrosion voltage of LC3 specimens with an inhibitor dosage of zero, RD and HD, respectively. Here, all the LC3 specimens showed more positive potential and zero macrocell corrosion current from an early age. Due to early hydration, the resistivity and strength gains are more in LC3 than in other binders. The microstructure evolves to finer pores inducing a tortuous path and preventing the ingress of chlorides to a negligible extent. The initial resistivity of the concrete will play a key role in establishing the type of circuit in ASTM G109 specimens [26]. The high resistivity of the LC3 concrete (See [Figure 13](#)) could induce Circuit 2 instead of Circuit 1 as the ionic conductivity is challenging to establish. This high resistivity of concrete needs attention as the electrochemical readings could be misleading. To investigate the LC3 specimen further, one specimen without inhibitor (S5) was autopsied. [Figure 11](#) shows the autopsied S5 specimen at about 500 days of exposure, where very minute rust spots along the length of the rebar were observed. However, such corrosion was not captured in the electrochemical reading due to the high ohmic drop associated with such highly resistive concrete. This observation indicates that the corrosion spots could be re-passivating even after formation as the resistivity is very high and the necessary electrolyte and ionic conduction are challenging to maintain. Moreover, the level of corrosion observed at 500 days of exposure was significantly less when compared to OPC and PFA specimens, which corroded earlier than 500 days, as per ASTM G109 standard (total current reaching 150 coulombs). Additionally, the corrosion products formed on the steel embedded in the LC3 system was very different (Hematite – with less expansive nature) and the study related to S-C interface has been discussed elsewhere [40]. In conclusion, the performance of LC3 specimens was superior to all other specimens tested, regardless of the presence of inhibitors. The corrosion initiation time in LC3 specimens was significantly delayed, about five times longer than that observed in PFA and OPC control specimens. Even though the addition of inhibitors in OPC and PFA specimens contributed to delaying the corrosion initiation time, LC3 control specimens outperformed them by a factor of two.

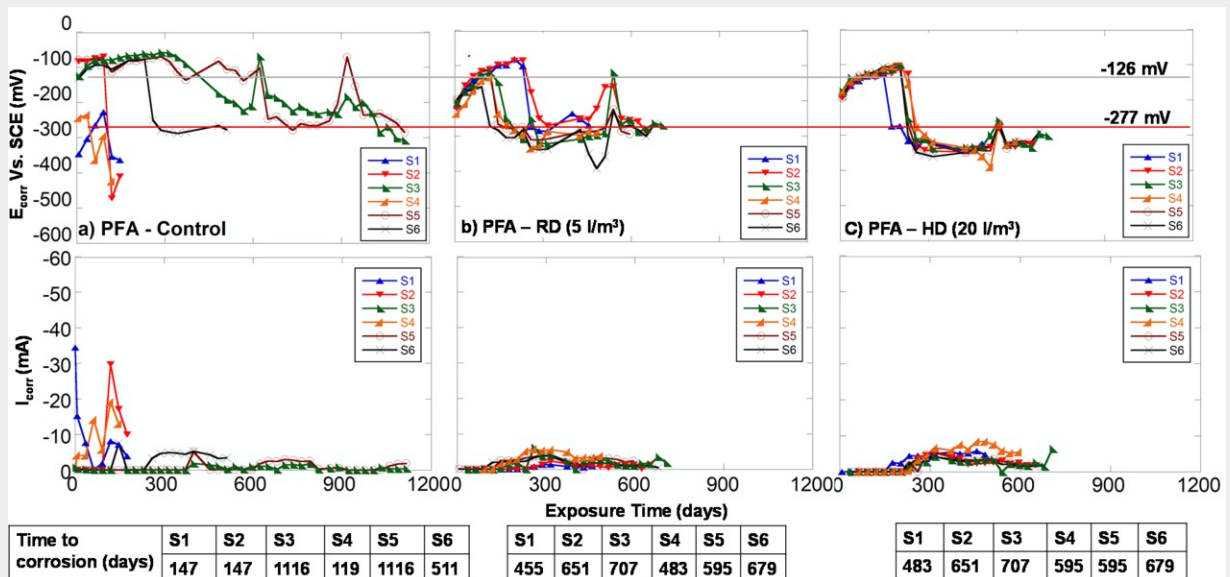
Figure 8. Possible Circuits in ASTM G109 specimens [38].



Note: Figure Replacement Requested.

Slide8Fig_F008.png

Figure 9. Half-cell potential and macrocell corrosion current of PFA – ASTM G109 specimens.



The half-cell potential of the top rebar indicates some corrosion activity whereas the macrocell corrosion was consistently zero or below zero, which confirms that Circuit 1 is not established. The testing of LC3 specimens was continued till 1100 days, where the specimens had no sign of corrosion from macrocell corrosion measurements. Based on the half-cell potential readings, it was decided to autopsy S6 specimens in all the three categories, which is shown in the [Figure 12](#). There were corrosion spots which were spatially distributed and could be visually observed in both LC3 control and LC3 RD specimens. Additionally, the corrosion observed in LC3-RD specimens were spread along the rebar compared to LC3 control. This could be due to the neutralizing effect of the inhibitor which could prevent pitting corrosion. Moreover, there was no indication of ongoing corrosion in macrocell corrosion current readings. This is because of the influence of the concrete resistivity in the measurement of ionic current established in Circuit 1 as explained earlier. Further, there were no spots found on LC3 HD specimens.

In general, LC3 specimens took significantly longer time for corrosion initiation than the corresponding OPC and PFA specimens with similar strength and mix design. However, such concretes with high resistivity and low alkalinity may have a high probability of pitting corrosion due to highly variable chloride penetration in a tortuous conductive path [29, 39]. Additionally, there was some surface scaling/crumbling (very minimal) observed in LC3 specimens. This could be due to salt crystallization in finer pores when subjected to wetting and drying and needs further study in the long run. It can be concluded that the type of binder and its resistivity play a vital role in the corrosion initiation time alone and susceptibility to pitting remains a concern for long term durability in highly resistive concretes. Therefore, a comprehensive understanding of the transport properties, corrosion mechanisms, and the overall condition of the concrete structure (presence of cracks, alkalinity, and various deterioration mechanisms) is necessary to accurately assess its long-term performance of a reinforced concrete structure ([Figure 10](#)).

Figure 10. Half-cell potential and macrocell corrosion current of LC3 – ASTM G109 specimens. +

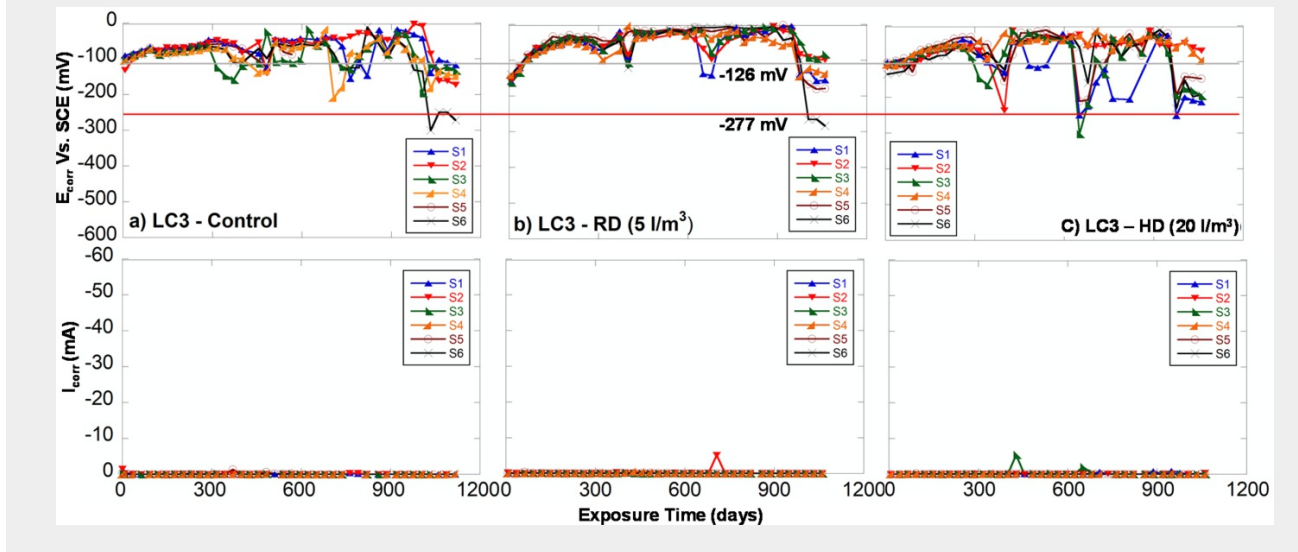
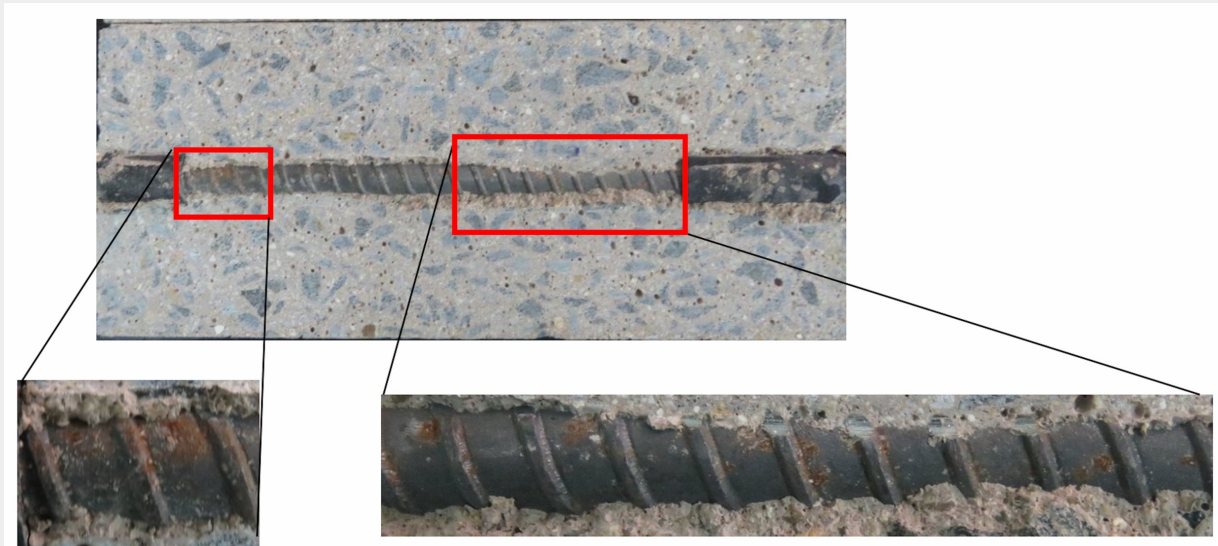
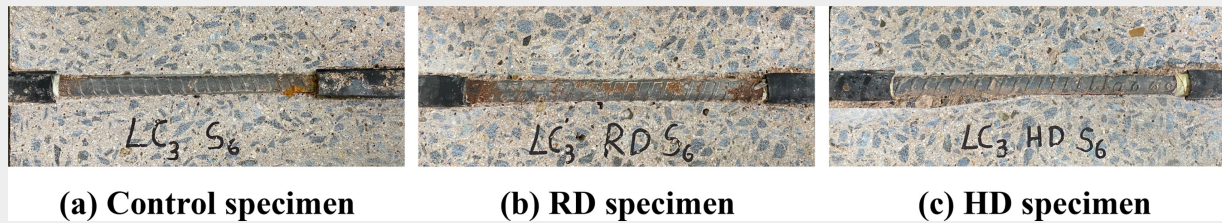


Figure 11. LC3 – S5 (Control specimen without inhibitor) at 500 days of testing. +



 Slide11Fig_F011.png

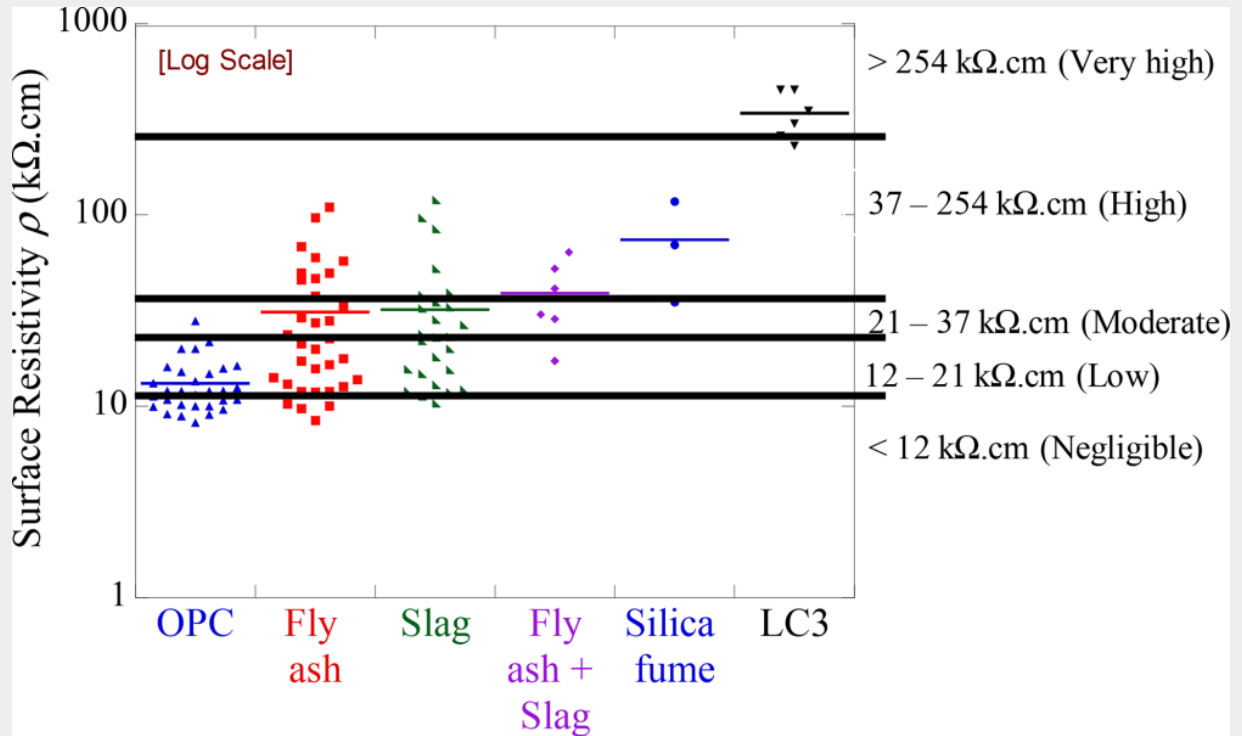
Figure 12. LC3 specimens cut after 1100 days of testing. +



4.3.1. Resistivity of concrete

The resistivity of concrete plays a significant role in establishing the electric and ionic circuits. In high resistivity concretes such as LC3, macrocell corrosion occurs within the rebar – Circuit 2 instead of Circuit 1, and the transport properties play a predominant role in the ingress of chlorides. This can be confirmed by the half-cell potential measurement, which provided clear indications of corrosion activity on the top rebar, whereas the macrocell current measurement did not show any signs of corrosion. However, until now, there is no clear indication in the literature about the resistivity range in which the ASTM G109 test method can indicate ongoing corrosion. Comparing the resistivity of concrete, the chloride resistance as per [1] and macrocell current, it can be concluded that the resistivity is predominant in establishing the Circuit and when surface resistivity (ρ) > 37 k Ω .cm at the time of testing, Circuit 2 can be predominant. Figure 13 shows the resistivity classification according to [1, 39]. When ρ > 37 k Ω .cm, as Circuit 2 could be predominant, the testing as per ASTM G109 will lead to erroneous conclusions due to the longer testing duration to assess the embedded steel's corrosion performance. To overcome this, it is recommended to use short-term test methods with mortar instead of concrete and with lesser cover to assess the electrochemical parameters. In addition, it is recommended to have specimens with single steel bar when assessing the electrochemical parameters and chloride induced corrosion in highly resistive binder systems. A lollipop test method alternative wetting and drying can be adopted to evaluate the long-term performance as described in 39.


Figure 13. Chloride resistance as per the surface resistivity of concretes [1, 39]. 

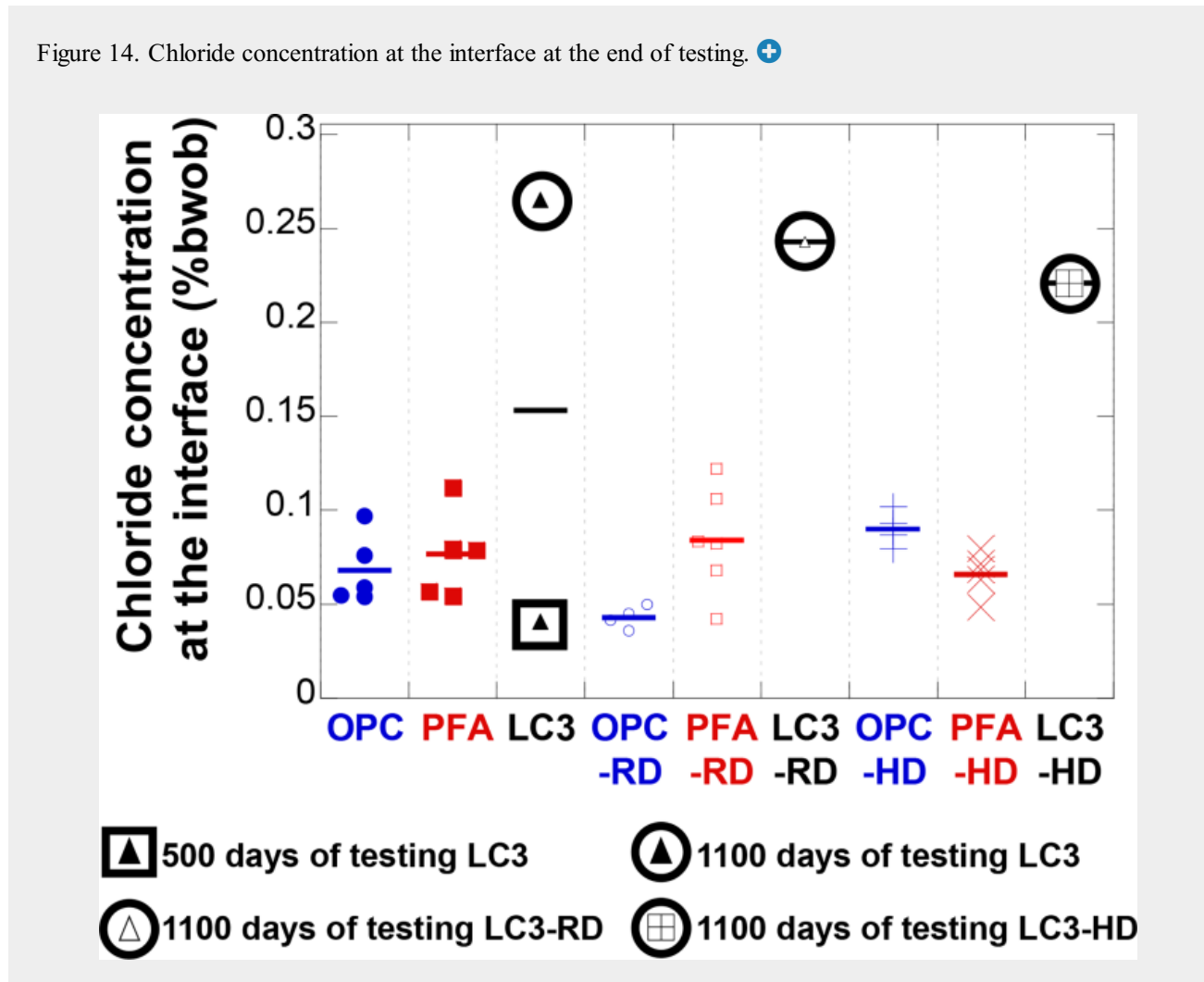


4.4. Chloride concentration at the interface

After autopsying, the chloride concentration at the S-C interface was determined by collecting the concrete powder from the region in contact with the steel bar and testing for acid-soluble chloride content in the powder. [Figure 14](#) shows the average chloride concentration at the interface. In OPC concrete, the presence of inhibitors played a significant role in the amount of chloride required to initiate corrosion and the time required. However, no significant changes in the chloride concentration are observed in PFA specimens. In general, the chloride concentration found is lesser than the typical values reported for the same S-C system in literature [4, 39]. This could be due to the stochastic nature of the chloride ingress through the preferential pathways such as capillary pores, voids, and microcracks in the concrete cover. Hence, the time of corrosion initiation depends on these pathways and is more influential than the actual diffusion co-efficient of the bulk cementitious matrix. In addition, when the chloride concentration is averaged through the exposure region, the interfacial chloride concentration found might have been a lesser value than the original value, which caused the corrosion initiation. So, it is recommended that while estimating service life, necessary precautions should be taken to consider this effect of preferential pathways. In addition, the chloride diffusion co-efficient averaged across the surface might lead to over-estimation. The uniform evolution of microstructure and refined pore structure are necessary to achieve the desired transport properties that can enhance the service life. It can be concluded that LC3 concrete had better

performance than its alternatives due to its better and refined microstructure throughout the matrix from a very early age.

Figure 14. Chloride concentration at the interface at the end of testing. 



4.5. Role of corrosion inhibitors

From the electrochemical readings and the time to initiation in each specimen, the OPC-control specimens exhibited the worst performance in severe chloride environments. In such cases, adding inhibitors would help, and more importantly, the dosage of the inhibitors can greatly influence the service life. However, in the case of slow-hydrating binders such as PFA, curing for sufficient duration to gain its full potential is also beneficial – along with adding corrosion inhibitors. On the other hand, highly resistive systems like LC3 had very high resistivity and uniform and denser matrix with refined microstructure and performed to its full potential against the ingress of chlorides. In such systems, resistivity plays a crucial role in establishing the circuit for the macrocell current (Circuit 1), and the critical failure criteria for the ASTM G109 test method, which is based on Circuit 1, cannot

always be achieved. In such cases, it is better to determine the surface resistivity of the concrete at 28 days and then decide on the test method. In addition, no significant difference was found in the corrosion initiation time when inhibitors were used along with SCM-based systems, especially in PFA specimens. It is, therefore, necessary that the admixtures should be tested in various S-C systems before site implementation. Though the chloride concentration required for corrosion initiation varies a lot from specimen to specimen, it is generally dependent on the interfacial properties when all other parameters, such as the type of steel and the concrete mix design are the same. These S-C interface properties can be regulated only by quality control. In general, the control of cover depth, compaction, and curing of concrete (3Cs) are strongly recommended to reduce the rate of ingress of chlorides and delay the corrosion initiation. [AQ2](#)

5. Conclusions

A comprehensive experimental program comprising six specimens for each combination of binder and inhibitor dosage was performed. The specimens were monitored for a period which defines the end of testing as per ASTM G109 or 1100 days whichever was earlier. A combination of visual and electrochemical readings was utilized to derive the following major conclusions.

1. LC3 has superior performance against chloride ingress and significantly better than the OPC and PFA specimens with a corrosion initiation time delay of five times. This is because of the high resistivity developed during the early stages of hydration and hence, the reduced rate of chloride ingress. However, susceptibility to pitting corrosion remains a concern, which can be mitigated by adding inhibitors.
2. The presence of corrosion inhibitors exhibited a significant effect on the corrosion initiation in OPC concretes, whereas its influence is minimal in PFA concretes. OPC concretes with high dosage of corrosion inhibitors outperformed PFA specimens with recommended and high dosages of corrosion inhibitors in terms of the time to corrosion initiation, exhibiting 30% improvement. It is worth noting that LC3 control specimens surpassed the performance of OPC and PFA specimens with inhibitors by a significant margin of two.
3. For highly resistive concretes, corrosion occurs predominantly in Circuit 2, which refers to the path between two points on the same bar. The ASTM G109 test method is not suitable for assessing the corrosion performance of steel in such concretes. A lollipop test specimen with an embedded rebar can be used for long term performance by subjecting it to alternative wet-dry cycle.

These findings highlight the importance of considering resistivity, corrosion inhibitors, and appropriate testing methods when evaluating the chloride resistance and corrosion performance of different cementitious systems. [AQ3](#)

Acknowledgements

The technical assistance by Ms. Keerthi V.T. and Ms. Sruthy Menon is kindly acknowledged. The authors also express their gratitude to the staff and researchers in the Construction Materials Research Laboratory (CMRL), Department of Civil Engineering, IITM, Chennai, India.

Disclosure statement




No potential conflict of interest was reported by the author(s). [AQ4](#)




Note: this Edit/html view does not display references as per your journal style. There is no need to correct this. The content is correct and it will be converted to your journal style in the published version.

References




- 1 [AASHTO T 358](#). Standard method of test for surface resistivity indication of concrete's ability to resist chloride ion penetration. Washington, DC (USA): American Association of State Highway and Transportation Officials; 2017. [+](#) [✎](#) [🗑](#)
- 2 [Alexander MG](#), [Beushausen H](#), [Otieno MB](#). 2013. Corrosion of steel in reinforced concrete: influence of cover cracking and concrete quality. Research Monograph No.9 in: guide to the Use of Durability Indexes for Achieving Durability in Concrete Structures, 1–77. [+](#) [✎](#) [🗑](#)
- 3 [Andrade PC](#), [Alonso C](#), [Polder R](#), et al. RILEM TC 154-EMC: electrochemical techniques for measuring metallic corrosion test methods for on-site corrosion rate measurement of steel reinforcement in concrete by means of the polarization resistance method. 2005;37:623–643. [+](#) [✎](#) [🗑](#)
- 4 [Angst UM](#), [Isgor OB](#), [Hansson CM](#), et al. Beyond the chloride threshold concept for predicting corrosion of steel in concrete. *Appl Phys Rev*. 2022;9(1):011321. doi: 10.1063/5.0076320. [+](#) [✎](#) [🗑](#)
- 5 [Angst UM](#), [Geiker MR](#), [Alonso MC](#), et al. The effect of the steel–concrete interface on chloride-induced corrosion initiation in concrete: a critical review by RILEM TC 262-SCI. *Mater Struct*. 2019;52(4). doi: 10.1617/s11527-019-1387-0. [AQ5](#) [+](#) [✎](#) [🗑](#)
- 6 [Angst UM](#), [Polder R](#). Spatial variability of chloride in concrete within homogeneously exposed areas. *Cem. Concr. Res*. 2014;56:40–51. 10.1016/j.cemconres.2013.10.010. [+](#) [✎](#) [🗑](#)
- 7 [Angst UM](#), [Ronnquist A](#), [Elsener B](#), et al. Probabilistic considerations on the effect of specimen size on the critical chloride content in reinforced concrete. *Corros Sci*. 2011;53(1):177–187. doi: 10.1016/j.corsci.2010.09.017. [+](#) [✎](#) [🗑](#)
- 8 [Arya C](#), [Vassie PR](#). Influence of cathode-to-anode area ratio and separation distance on galvanic corrosion




currents of steel in concrete containing chlorides. *Cem Concr Res.* 1995;25(5):989–998. doi: 10.1016/0008-8846(95)00094-S.   




9 ASTM C1202-22E1. 2022. Standard test method for electrical indication of concrete's ability to resist chloride ion penetration. Conshohocken, (PA): American Society of Testing and Materials. doi: 10.1520/C1202-22E01.   




10 ASTM C1556-04. 2010. Standard test method for determining the apparent chloride diffusion coefficient of cementitious mixtures by bulk diffusion. Conshohocken, (PA): American Society of Testing and Materials.   




11 ASTM C876-15. 2015. Standard test method for corrosion potentials of uncoated reinforcing in concrete. West Conshohocken, (PA): ASTM International.   

12 ASTM G109-07. 2013. Standard test method for determining effects of chemical admixtures on corrosion of embedded steel reinforcement in concrete exposed to chlorides. West Conshohocken (PA): ASTM International.   




13 ASTM G180-13. 2014. Standard test method for corrosion inhibiting admixtures for steel in concrete by polarization resistance in cementations slurries. Conshohocken, (PA): American Society of Testing and Materials.   




14 Avet F, Scrivener K. Influence of pH on the chloride binding capacity of limestone calcined clay cements (LC3). *Cem Concr Res.* 2020;131(March):106031–106370. doi: 10.1016/j.cemconres.2020.106031.   

15 Avet F, Snellings R, Alujas A, et al. Development of a new rapid, relevant and reliable (R3) testing method to evaluate the pozzolanic activity of calcined clays. *Cem Concr Res.* 2016;85:1–11. doi: 10.1016/j.cemconres.2016.02.015.   

16 Berke NS, Shen DF, Sundberg KM. Comparison of the polarization resistance technique to the macrocell corrosion technique. In: N S Berke, V Chaker, and D Whiting, editors. *Corrosion rates of steel in concrete*, ASTM STP 1065. Philadelphia: American Society for Testing and Materials; 1990. p. 38–51.   

17 Boubitsas D, Tang L. An approach for measurement of chloride threshold values. *IJSTRUCTE.* 2013;4(1/2):24–34. doi: 10.1504/IJSTRUCTE.2013.050762.   

18 Dhandapani Y, Santhanam M. Assessment of pore structure evolution in the limestone calcined clay cementitious system and its implications for performance. *Cem Concr Compos.* 2017;84:36–47. doi: 10.1016/j.cemconcomp.2017.08.012.   

19 Dhandapani Y, Sakthivel T, Santhanam M, et al. Mechanical properties and durability performance of concretes with limestone calcined clay cement (LC3). *Cem Concr Res.* 2018;107(March):136–151. doi: 10.1016/j.cemconres.2018.02.005.   

- 20 ~~Wedding PA~~, Diamond S. Chloride concentrations in concrete pore solutions resulting from calcium and sodium chloride admixtures. *Cement, Concrete, Aggr.* 1986;8(2):97–102. doi: 10.1520/CCA10062J.   
- 21 Elsener B. Half-cell potential mapping to assess repair work on RC structures. *Constr Build Mater.* 2001;15(2–3):133–139. doi: 10.1016/S0950-0618(00)00062-3.   
- 22 Elsener B. Macrocell corrosion of steel in concrete – Implications for corrosion monitoring. *Cem Concr Compos.* 2002;24(1):65–72. doi: 10.1016/S0958-9465(01)00027-0.   
- 23 Emmanuel AC, Haldar P, Maity S, et al. Second pilot production of limestone calcined clay cement in India: the experience. *Indian Concrete J.* 2016;90:57–63.   
- 24 Figueira RB, Sadovski A, Melo AP, et al. Chloride threshold value to initiate reinforcement corrosion in simulated concrete pore solutions: the influence of surface finishing and pH. *Constr Build Mater.* 2017;141:183–200. doi: 10.1016/j.conbuildmat.2017.03.004.   
- 25 Elsener B, Andrade C, Gulikers J, et al. Half-cell potential measurements –potential mapping on reinforced concrete structures. *Mat Struct.* 2003;36(7):461–471. doi: 10.1007/BF02481526.   
- 26 Hansson CM, Poursaeed A, Laurent A. Macrocell and microcell corrosion of steel in ordinary Portland cement and high performance concretes. *Cem Concr Res.* 2006;36(11):2098–2102. doi: 10.1016/j.cemconres.2006.07.005.   
- 27 Krishnan S, Bishnoi S. Understanding the hydration of dolomite in cementitious systems with reactive aluminosilicates such as calcined clay. *Cem Concr Res.* 2018;108(March):116–128. doi: 10.1016/j.cemconres.2018.03.010.   
- 28 Li L, Sagues AA. Effect of chloride concentration on the pitting and repassivation potentials of reinforcing steel in alkaline solutions. *Nace Corrosion.* 1999;567(567). [AQ6](#)   
- 29 Li C, Xiao K. Chloride threshold, modelling of corrosion rate and pore structure of concrete with metakaolin addition. *Constr Build Mater.* 2021;305:124666. doi: 10.1016/j.conbuildmat.2021.124666.   
- 30 Liu G, Zhang Y, Ni Z, et al. Corrosion behavior of steel submitted to chloride and sulphate ions in simulated concrete pore solution. *Constr Build Mater.* 2016;115:1–5. doi: 10.1016/j.conbuildmat.2016.03.213.   
- 31 Lollini F, Redaelli E, Bertolini L. Investigation on the effect of supplementary cementitious materials on the critical chloride threshold of steel in concrete. *Mater Struct.* 2016;49(10):4147–4165. doi: 10.1617/s11527-015-0778-0.   
- 32 Mammoliti L, Hansson CM, Hope BB. Corrosion inhibitors in concrete part II: effect on chloride threshold values for corrosion of steel in synthetic pore solutions. *Cem Concr Res.* 1999;29(10):1583–1589. doi: 10.1016/S0008-8846(99)00137-4.   

- 33 Maraghechi H, Avet F, Wong H. et al. Performance of Limestone Calcined Clay Cement (LC3) with various kaolinite contents with respect to chloride transport. *Mater Struct* (2018);51:125. <https://doi.org/10.1617/s11527-018-1255-3> ~~Mater. Struct. 2018;~~   
- 34 NT Build 443. Concrete, hardened: accelerated chloride penetration. In: *Nordtest method*. Finland: ESPOO; 1995.   
- 35 NT Build 492. Concrete, mortar and cement-based repair materials: chloride migration coefficient from non-steady-state migration experiments. In: *Nordic Council of Ministers*. Finland: UDC; 1999.   
- 36 Ogunsanya IG, Hansson CM. Detection of the critical chloride threshold of carbon steel rebar in synthetic concrete pore solutions. *RILEM Tech Lett*. 2019;3(2018):75–83. doi: 10.21809/rilemtechlett.2018.70.   
- 37 Pour-Ghaz M, Isgor OB, Ghods P. Quantitative interpretation of half-cell potential measurements in concrete structures. *J Mater Civ Eng*. 2009;21(9):467–475. doi: 10.1061/(ASCE)0899-1561(2009)21:9(467). [AQ7](#)   
- 38 Rengaraju S, Godara A, Alapati P, et al. Macrocell corrosion mechanisms of prestressing strands in various concretes. *Magazine Concrete Res*. 2020;72(4):194–206. doi: 10.1680/jmacr.18.00284.   
- 39 Rengaraju S, Pillai RG. An accelerated chloride threshold test for uncoated steel in highly resistive cementitious systems (hr-ACT test). *Constr Build Mater*. 2021;305:124797. doi: 10.1016/j.conbuildmat.2021.124797.   
- 40 Rengaraju S, Pillai RG, Gettu R, et al. Effect of test methods on corrosion phenomena of steel in highly resistive concrete systems and data interpretations. *Nace Corrosion*. 2021;77(4):445–459. doi: 10.5006/3705.   
- 41 RILEM TC 235-CTC. 2014. Technical committee corrosion initiating chloride threshold concentrations in concrete. Available from: <https://www.rilem.net/groupe/235-ctc-corrosion-initiating-chloride-threshold-concentrations-in-concrete-237>.   
- 42 Saremi M, Mahallati E. A study on chloride-induced depassivation of mild steel in simulated concrete pore solution. *Cem Concr Res*. 2002;32(12):1915–1921. doi: 10.1016/S0008-8846(02)00895-5.   
- 43 Scrivener KL. 202 Special Issue – Options for the future of cement. *Indian Concrete J*. 2014;88(7):11–21. doi: 10.1002/(SICI)1097-0045(19990501)39:2 < 108::AID-PROS5 > 3.0.CO;2-9.   
- 44 Scrivener KL, John VM, Gartner EM. Eco-efficient cements: potential economically viable solutions for a low-CO₂ cement-based materials industry. *Cem Concr Res*. 2018;114(June):2–26. doi: 10.1016/j.cemconres.2018.03.015.   
- 45 SHRP-330. Standard test method for chloride content in concrete using the specific ion probe. In: *Condition evaluation of concrete bridges relative to reinforcement corrosion – volume 8: procedure manual, SHRP-S/FR-92-110*. Washington, DC (USA): *Strategic Highway Research Program*; 1993. p. 85–105. [AQ8](#)   

46 Yu H, Chiang KTK, Yang L. Threshold chloride level and characteristics of reinforcement corrosion initiation in simulated concrete pore solutions. *Constr Build Mater.* 2012;26(1):723–729. doi: 10.1016/j.conbuildmat.2011.06.079. [AQ9](#)[AQ10](#)   

Author Query

1. **Query [AQ0]** : Please review the table of contributors below and confirm that the first and last names are structured correctly and that the authors are listed in the correct order of contribution. This check is to ensure that your names will appear correctly online and when the article is indexed. ↑

Sequence	Prefix	Given name(s)	Surname	Suffix
1		Sripriya	Rengaraju	
2		Radhakrishna	G. Pillai	

Response by Author: "Ok"

2. **Query [AQ1]** : Please confirm whether the affiliations and corresponding details presented are appropriate, amend if necessary. ↑

Response by Author: "Ok"

3. **Query [AQ2]** : Please check and approve whether the insertion of citation for Figure 10 is appropriate. ↑

Response by Author: "The citation is in wrong place. It should be Figure 10 (a-c) instead of Figure 8(a-c) just after the subheading 4.3 LC3 specimens. I updated the text"

4. **Query [AQ3]** : Please confirm whether hierarchy of section headings is appropriate and amend if necessary. ↑

Response by Author: "Ok"

5. **Query [AQ4]** : Please confirm whether the "Disclosure Statement" is appropriate, amend if necessary. ↑

Response by Author: "Ok"


6. **Query [AQ5]** : Please provide missing page range for the "Angst et al., 2019 (Ref. 5). " references list entry. ↑

Response by Author: "It does not have page range"


7. **Query [AQ6]** : Please provide missing page range for the "Li and Sagues, 1999 (Ref. 27). " ↑

references list entry.


Response by Author: "It does not have page range"

8. **Query [AQ7]** : The year of publication has been changed as per Crossref details both in the list and in the text for this reference. Please check. 


Response by Author: "ok. The reference is also updated"

9. **Query [AQ8]** : Name and date citations have been changed into numbered citations. Please check whether the citations have been replaced safety. 


Response by Author: "Ok"

10. **Query [AQ9]** : Please provide complete details for (Gulikers et al. 2003; Diamond, 1986; Angst and Polder, 2014; Maraghechi et al. 2019) in the reference list or delete the citation from the text. 

Response by Author: "1) Gulikers et al.2003 should be Elsener et al. 2003 and is reference 24. IT is also updated in the text2)Diamond 1986 is reference 19. The reference is updated3) Add reference for Angst and Polder 2014 as U.M. Angst, R. Polder, Spatial variability of chloride in concrete within homogeneously exposed areas, Cem. Concr. Res. 56 (2014) 40–51. <https://doi.org/10.1016/j.cemconres.2013.10.010>.4) Correct the year in Maraghechi et al.2019 as 2018 and add reference asMaraghechi, H., Avet, F., Wong, H. et al. Performance of Limestone Calcined Clay Cement (LC3) with various kaolinite contents with respect to chloride transport. Mater Struct 51, 125 (2018). <https://doi.org/10.1617/s11527-018-1255-3>"

11. **Query [AQ10]** : There is no mention of Reference [3, 5, 8, 9, 10, 11, 19, 24, 32, 33, 39, 43] in the text. Please insert a citation in the text or delete the reference as appropriate, maintaining the numerical order of the references. 

Response by Author: "RILEM 9 TC 154-EMC in the text is ref. 3; RILEM TC 262-SCI in the text is ref. 5; ASTM C1202 in the text is ref.8;ASTM C1556 in the text is ref.9; ASTM C876 in the text is ref.10; ASTM G109 is ref.11; Diamond (1984) is ref. 19; Ref.24 is corrected in the text as Elsener et al.2003; NT Build 443 in the text is ref. 32; NT Build 492 in the text is ref. 33; RILEM TC 235-CTC in the text is ref.39; SHRP-330 in the text is ref.43."

12. **Query [AQ11]** : Please note that Figure 6, 8, and 9 subparts "a–c" have been cited in the text but the explanation text for these subparts are missing in Figure 6, 8, and 9 caption. Please check 

and update.

Response by Author: "The subparts for figures 6, 9, and 10 are mentioned in the figure itself and not in the caption. There is no subpart for figure 8."

Figure Replacement

1.

Figure 11. replaced by Author:

'F011.png' replace to 'Slide11Fig_F011.png'

Note: This figure cannot be displayed here due to it being a big size or not supporting the format.

2.

Figure 5. replaced by Author:

'F005.png' replace to 'Slide5Fig_F005.png'

Note: This figure cannot be displayed here due to it being a big size or not supporting the format.

3.

Figure 8. replaced by Author:

'F008.png' replace to 'Slide8Fig_F008.png'

